Composition dependence of metallic glass plasticity and its prediction from anelastic relaxation – a shear transformation zone analysis

T. J. Lei[1], L. Rangel DaCosta[1], M. Liu[2], J. Shen[2], Y. H. Sun[2], W. H. Wang[2] and M. Atzmon[1,3,*]

[1] Department of Materials Science and Engineering, University of Michigan, Ann Arbor, Michigan, 48109, USA.

[2] Institute of Physics, Chinese Academy of Sciences, Beijing, 100190, China.

[3] Department of Nuclear Engineering and Radiological Sciences, University of Michigan, Ann Arbor, Michigan, 48109, USA.

[*] Corresponding author: atzmon@umich.edu

Abstract

The mechanical relaxation behavior of metallic glasses (MGs) is composition sensitive. For example, in dynamic mechanical analysis, $La_{70}Ni_{15}Al_{15}$ shows a pronounced secondary peak, termed β relaxation, of the normalized loss modulus at high frequency and/or low temperature, while $La_{70}Cu_{15}Al_{15}$ only exhibits a shoulder. We have determined relaxation-time spectra at room temperature for these alloys over eleven orders of magnitude of time from quasi-static anelastic relaxation measurements. These are employed to characterize shear transformation zone (STZ) properties in both the α and β regimes. The pronounced β relaxation peak, observed for $La_{70}Ni_{15}Al_{15}$, is a result of *both* larger volume fraction of fast and small *potential* STZs *and* smaller volume fraction of slow and large *potential* STZs as compared to $La_{70}Cu_{15}Al_{15}$. Room-temperature tensile tests show increasing plasticity with decreasing strain rates, characteristic of thermally activated processes. $La_{70}Cu_{15}Al_{15}$ exhibits greater plasticity than $La_{70}Ni_{15}Al_{15}$, a negative correlation with the intensity of the β relaxation that is opposite to that previously suggested. The STZ spectra are used to explain the plasticity difference between the two alloys. Plasticity predictions from loss modulus measurements need to be revised, and require absolute measurements.

Introduction and background

The strength of metallic glasses (MGs) is significantly higher than that of polycrystals with comparable composition [1]. However, structural applications of MGs are often restricted by their limited macroscopic plasticity, resulting from strain localization within dominant shear bands due to shear softening [2,3]. Recently, MG plasticity has been correlated with the intensity of the secondary (β) relaxation in normalized loss modulus data at high frequency and/or low temperature [4]. For some MGs, the β relaxation manifests as an "excess wing" [5]. Yu *et al.* [6] reported on a La-based MG with a distinct and pronounced β relaxation peak, which also exhibits relatively large tensile ductility. They argued, as they also do in Ref. [7], that the β relaxation is a manifestation of the activation of shear transformation zones (STZs, [8,9]), implying that the α relaxation corresponds to a different mechanism. However, Ju and Atzmon [10,11,12] and Lei *et al.* [13] showed that both α and β relaxations can be explained by the STZ model. While α vs. β relaxation in molecular glasses have been attributed to inter- vs. intramolecular motion, such a distinction cannot be made in MGs, posing a challenge in the identification of the relaxation mechanisms.

The chemical composition can significantly affect the intensity of the β relaxation. For example, the alloy systems La-Cu-Al and La-Ni-Al have similarly wide supercooled liquid region [14,15], but exhibit dramatically different β relaxation behavior – by substituting Ni with Cu, which has a similar atomic size, the strong β peak diminishes to an "excess wing" [16]. Yu *et al.* [17] speculated that large, similar, negative pairwise enthalpy of mixing among all constituting atoms results in a pronounced β relaxation, while positive or significantly varying values suppress the β relaxation and are usually associated with an "excess wing". This correlation is consistent with the $La_{70}(Cu_xNi_{1-x})_{15}Al_{15}$, x=0,1 system and offers a semi-quantitative way to predict the β relaxation.

However, the microscopic origin of the composition effect on relaxation behavior has yet to be elucidated.

In previous work by Ju *et al.* [12], an atomically quantized hierarchy of STZs was resolved in anelastic relaxation-time-spectra of an Al-rich MG – these exhibited a series of distinct peaks, the analysis of which indicated correspondence to a single-atomic volume increment. We later characterized the effects of cryogenic cycling and room temperature (RT) aging on properties of slow and large STZs, corresponding to the α relaxation, for $La_{70}(Cu_xNi_{1-x})_{15}Al_{15}$, x=0,1 MGs, resolved by STZ size [18].

The STZ concept has been used in the literature with varying meanings, which motivates us to clarify the terms used in this and our previous work. In his pioneering work [8], Argon defined a shear transformation as a "stress-activated structural transformation around a fertile site containing liquid-like sites" [19], and analyzed its thermally-activated dynamics. Falk and Langer [9] defined shear transformation zones as "small regions,… susceptible to inelastic rearrangements in response to shear stresses". They assumed the shear transformation zone to have two stable states, and only considered the zero-temperature, i.e., athermal, limit. In essence, both assume the existence of regions prone to shear transformations. In our past and present work, the term "STZ" refers to a cluster of atoms that has undergone a shear transformation, whereas a *potential* STZ (PSTZ) is a cluster capable of undergoing a shear transformation. Since we observe that the strain, even that associated with time constants greater than 6×10^7 s, is fully reversible [18], we consider it reasonable to employ, for a given direction of the shear stress, a two-state model. We further adopt the kinetic model of Ref. [8] to a spectrum of STZs, with a well-defined meaning attributed to the

pre-exponential factor: each spectrum peak is attributed to a distinct STZ type, indexed with *m*. If the volume fraction occupied by PSTZs of type *m* is c_m, under an applied shear stress σ, their transformations' contribution to the shear strain rate is given by [12],

$$\dot{\gamma}_m = 2c_m\gamma_o^c\nu_G \exp\left(-\frac{\Delta F_m}{kT}\right)\sinh\left(\frac{\sigma\gamma_o^T\Omega_m}{2kT}\right), \quad (1)$$

where γ_0^T is the unconstrained transformation shear strain ($\approx$ 0.2 [12]), and $\gamma_0^c = [2(4-5\nu)/15(1-\nu)]\gamma_0^T$ is the constrained value with $\nu = 0.324$ [20] being Poisson's ratio. ν_G is the attempt frequency, *k* is Boltzmann constant, and *T* is the temperature. Ω_m is the *m*-type STZ volume, and $\gamma_o^T\Omega_m$ is the activation volume. ΔF_m is the activation free energy for shear transformation of *m*-type STZs [12,21],

$$\Delta F_m = \left[\left(\frac{(7-5\nu)}{30(1-\nu)} + \frac{2(1+\nu)}{9(1-\nu)}\bar{\beta}^2\right)\gamma_0^T + \frac{1}{2}\frac{\overline{\sigma_{STZ}}}{\mu}\right]\mu\gamma_0^T\Omega_m, \quad (2)$$

where $\bar{\beta}^2 \sim 1$ is the dilatancy factor. $\overline{\sigma_{STZ}}$ is the shear resistance of STZs, μ is the shear modulus, and $\overline{\sigma_{STZ}}/\mu = 0.025$ [22]. In Ref. [8], in contrast, the pre-exponential factor for the total strain rate is described as a number of the order of 0.5, which depends on the density of fertile sites. In our work, the c_m are obtained from mechanical equilibrium [12], and therefore their uncertainty is far smaller than that in pre-exponential factors obtained, e.g., from temperature-dependent kinetic data.

The present work focuses on the composition effect on both α and β relaxations, by comparing the properties of *both* slow and large *and* fast and small STZs, with time constants spanning eleven

orders of magnitude, between $La_{70}Cu_{15}Al_{15}$ and $La_{70}Ni_{15}Al_{15}$. By computing relaxation-time spectra from quasi-static anelastic relaxation data, we achieve far better resolution of the relaxation processes than in dynamic mechanical analysis (DMA). When assuming a uniform shear modulus, two regimes of STZ activation volume are obtained, similar to a previously studied, different, La-based MG [13]. Spatial variation of the modulus [23,24] could provide an alternative interpretation. The pronounced β relaxation, observed in the normalized loss modulus vs. temperature or frequency for $La_{70}Ni_{15}Al_{15}$ but not for $La_{70}Cu_{15}Al_{15}$, is a result of two contributions – the former contains a larger volume fraction of fast and small PSTZs and a smaller volume fraction of slow and large PSTZs. In RT tensile tests, the plasticity of $La_{70}Cu_{15}Al_{15}$ is much larger than that of $La_{70}Ni_{15}Al_{15}$, indicating that a correlation between a pronounced β relaxation and large macroscopic plasticity [6] is not universal.

As pointed out by Orowan [25] and later by Argon [8], the shear transformation mechanism describes both anelastic and permanent deformation. Small strain, with corresponding small STZ concentration, can be reversed in a time-dependent manner by back-stress in the elastic matrix. With increasing strain and STZ concentration, back stress is lost, resulting in permanent strain. In agreement with this picture, we show the observed anelastic spectra to be qualitatively consistent with the plasticity results, suggesting a predictive potential of simple quasi-static anelasticity measurements.

Experimental and analysis details

The main details are reviewed here, and for further information, the reader is referred to Refs. [12,13,18]. Amorphous $La_{70}Cu_{15}Al_{15}$ and $La_{70}Ni_{15}Al_{15}$ (at.%) ribbons ~ 40 μm thick and 1 mm

wide were obtained by single-wheel melt-spinning under the same condition as Ref. [18]. Their glass transition temperatures are 391 K and 431 K [16], respectively. Samples were stored at room temperature (RT), 293±1 K, in argon-gas environment in order to prevent oxidation, except when retrieved for measurements. The amorphous structure was confirmed by X-ray diffraction. Samples were aged at RT for $1.9 \cdot 10^6$ s before RT anelastic relaxation measurements. The anelastic strain vs. time data were obtained from a combination of two measurement techniques [12,13] – 1) nanoindenter bending of 1 mm long cantilevers using Hysitron TI950 TriboIndenter for 200 s, by applying a fixed load of 200 μN and monitoring the corresponding vertical displacement, and 2) constraint-free bend relaxation ("mandrel") measurements from ~ 20 s to $5.35 \cdot 10^7$ s, by monitoring the evolution of radius of curvature after a sample is constrained around a mandrel of radius 0.35 cm for $t_c = 2 \cdot 10^6$ s. For cantilever bending, each alloy was investigated by using three samples with 20 runs for each. For mandrel measurements, three samples for $La_{70}Cu_{15}Al_{15}$ and four samples for $La_{70}Ni_{15}Al_{15}$ were examined. The strain at the surface, and next to the clamp for the cantilever, was calculated following Ref. [12]. The macroscopic plasticity was determined using RT tensile tests with a TA Instruments Q800 Dynamic Mechanical Analyzer, using a gauge length of 1 cm. Engineering strain rates of 10^{-4} s^{-1}, 10^{-5} s^{-1} and $1.6 \cdot 10^{-6}$ s^{-1} were used, with samples of similar ageing times. Three samples were tested for each alloy and strain rate.

As in Refs. [12,13,18], relaxation-time spectra, $f(\tau)$, were computed from the normalized anelastic strain vs. time data by employing a standard linear solid model [26]. A portable package for inverse problems, CONTIN [27,28], was used [13,18], which yields stable and consistent fitting of the anelastic strain. To approximate a continuous spectrum without making assumptions on its shape or number of processes it reflects, a large number of fixed, logarithmically spaced relaxation-time

values (τ_i) are used: 100 from 0.0015 s to 400 s and 50 from 10 s to $1.07 \cdot 10^8$ s for cantilever bending and mandrel measurements, respectively. The number of spectrum points is always smaller than the number of data points. To eliminate unphysical spectrum peaks due to numerical artifacts, a regularization term was included in nonlinear least-squares fitting during CONTIN computation [27,28], and similar regularization parameter values were used for all samples for consistency. Details on spectrum computation and consistency checks are provided in Refs. [12,13,18]. Spectrum peak properties were determined as the average over all samples of the same composition, and the random error was estimated from the standard deviation of the mean.

Results

Figure 1 shows the anelastic strain, normalized by the equilibrium elastic strain, vs. time, obtained from both measurement techniques, for each alloy after a prior RT aging time of $1.9 \cdot 10^6$ s. For cantilever bending (Fig. 1a), an average curve of all tests is shown for each alloy. Due to the large number of data points (~ 60000) for each run, each point in Fig. 1a is an average of 500 data points. The elastic strain was determined from the instantaneous displacement, about 1500 nm for the geometry used. The anelastic displacement reached 110-180 nm after 200 s. For the mandrel measurements (Fig. 1b), data corresponding to all samples are displayed, showing the degree of reproducibility. At short measurement time (Fig. 1a), $La_{70}Ni_{15}Al_{15}$ shows higher strain magnitude than $La_{70}Cu_{15}Al_{15}$, with a much larger slope from 0.1 s to ~5 s, observed consistently for all samples. The behavior at longer time (Fig. 1b), after constraint removal, is discussed in detail in Ref. [18] in the context of the effects of RT aging and cryogenic cycling, and is briefly reviewed here: 1) the anelastic strain magnitude is much higher for $La_{70}Cu_{15}Al_{15}$ than for $La_{70}Ni_{15}Al_{15}$, opposite to the short-time behavior; 2) the absolute strain relaxation rate up to 10^4 s ~ 10^5 s is

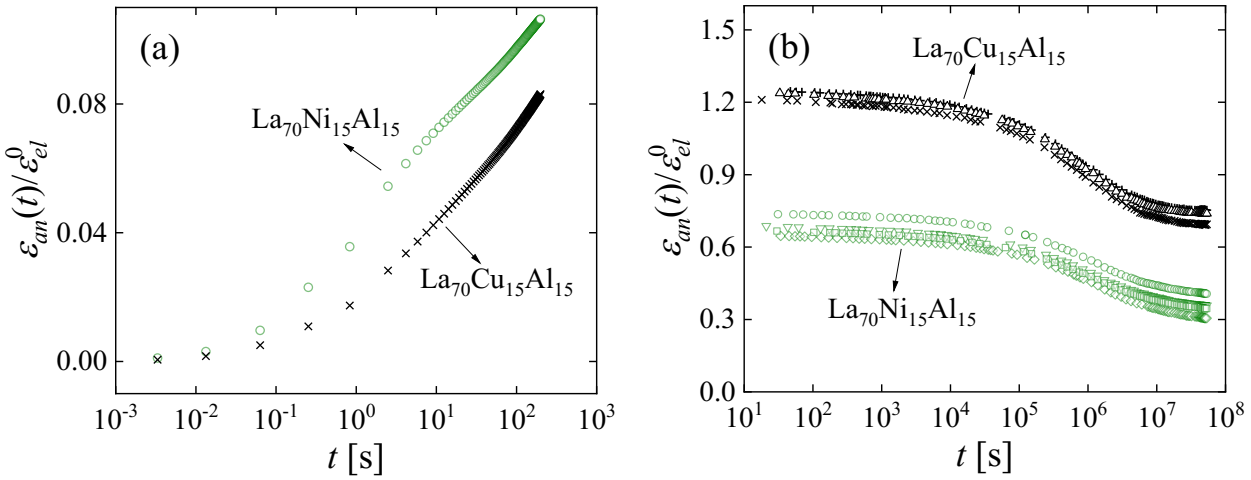

Figure 1. Anelastic strain, normalized by the corresponding equilibrium elastic strain, vs. time for (a) cantilever bending and (b) mandrel measurements for $La_{70}Cu_{15}Al_{15}$ and $La_{70}Ni_{15}Al_{15}$ with a prior RT aging time of $1.9 \cdot 10^6$ s. For cantilever bending, an average of all tests for the same composition is displayed, and each point is an average of 500 experimental data points. For the mandrel measurements, data corresponding to all samples are shown.

similar for both alloys, but differs at longer time. This implies that the difference in the strain magnitude is mainly due to the large-time-constant processes, 3) the measured strain is purely anelastic, as verified by its full reversal by annealing.

Figure 2 shows the relaxation-time spectra computed from the strain evolution data of Fig. 1. Similar to Fig. 1, for the cantilever bending, an average spectrum over all tests is shown for each alloy, and it is noted that the spectrum shape is the same for all samples and runs for each composition. For the mandrel measurements, all spectra are shown. Reference [18] focused on the effect of structural relaxation and cryogenic rejuvenation on large-time-constant spectra for $La_{70}Cu_{15}Al_{15}$ and $La_{70}Ni_{15}Al_{15}$. Presently, we focus on the chemical composition effect on both

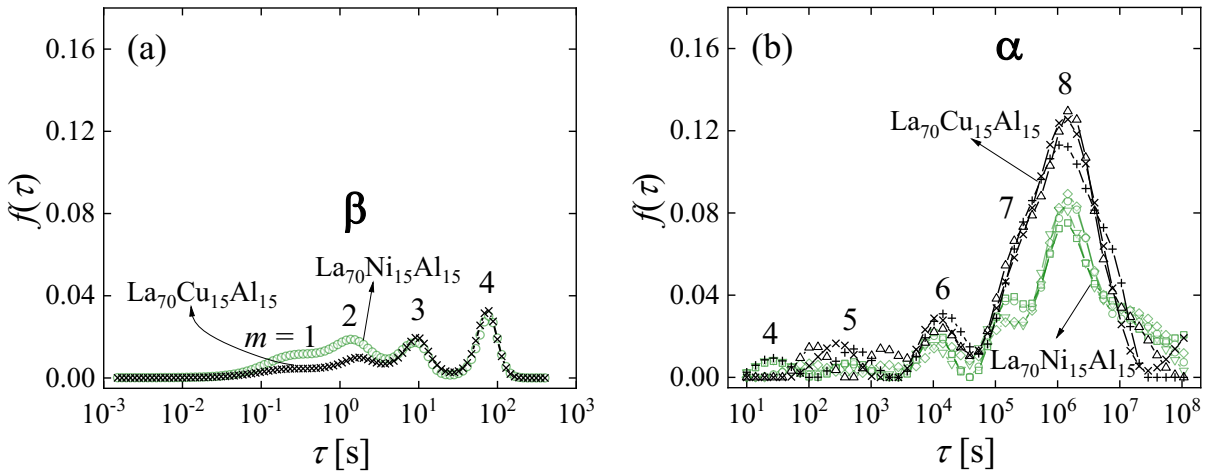

Figure 2. Relaxation-time spectra for (a) cantilever bending and (b) mandrel measurements, computed from the normalized anelastic strain vs. time data of Fig. 1 for $La_{70}Cu_{15}Al_{15}$ and $La_{70}Ni_{15}Al_{15}$ aged at RT for $1.9 \cdot 10^6$ s. For cantilever bending, an average of all spectra is shown for each alloy, and the standard deviation of the mean is smaller than the symbols. All spectra are presented for the mandrel measurements. Peaks are numbered m=1,…,8, corresponding to different STZ types. See text for identification of the α and β regimes.

small- and large-time-constant spectra for these two alloys. Similar to our previous studies [12,13,18], all spectra consist of distinct peaks. Based on a standard linear solid model [26], these peaks are associated with different STZ types, labeled m = 1,…,8. As mentioned in Ref. [13], the last peak from the nanoindenter cantilever and the first peak from the mandrel measurements should correspond to the same STZ type, m = 4. However, the different intensities are possibly due to the inability of the standard linear solid model to fully capture the strain-magnitude difference between fixed-load and constraint-free relaxation.

We attribute the different regimes in Fig. 2 (and Fig. 3 below) a vs. b to β vs. α relaxations, based on a) the trends in the peak areas across the range of time constants, discussed below, and b) extrapolation of published dynamic data [29], using the temperature dependence of the time constants [12], also detailed below in Eq. (4). In dynamic-mechanical analysis, a relaxation process with time constant τ contributes to the loss modulus $E''(\omega)$ at fixed temperature a Cauchy function that peaks at $\omega = 2\pi f = 1/\tau$, where f is the frequency. Integration (Refs. [10,11]) relates $f(\tau)$ to $E''(\omega)$. For $La_{70}Ni_{15}Al_{15}$, extrapolation of the β peak position of 330 K at $f = 1$ Hz [29] to room temperature shows that it originates from $m \leq 3$ STZs.

In Fig. 2, the peak positions are similar for both alloys, but their intensities are very different. At small time constants, from ~ 0.1 s to 5 s, corresponding to the β relaxation, the peak intensity is significantly higher in $La_{70}Ni_{15}Al_{15}$ than in $La_{70}Cu_{15}Al_{15}$. This difference was observed consistently for all three samples of each composition, and the standard deviation of the displayed mean is smaller than the symbols. This difference is consistent with the slope difference in Fig. 1a from $t \sim 0.1$ s to 5 s. At larger time constants, especially for $t > 10^5$ s, which corresponds to the slower α relaxation, the peak intensity is much higher for $La_{70}Cu_{15}Al_{15}$ than for $La_{70}Ni_{15}Al_{15}$. As shown in Ref. [12], the integrated area of peak m is equal to the pre-factor in Eq. (1), the volume fraction occupied by PSTZs of the corresponding type,

$$c_m = \int_m f(\tau) \mathrm{d}\ln\tau. \tag{3}$$

By definition [12], this integrated peak area is also equal to the normalized anelastic strain corresponding to Peak m. The intensity of the β relaxation is typically discussed based on loss

modulus plots, in which the maximum of the α relaxation is normalized to 1. For example, a pronounced β peak is identified in $La_{70}Ni_{15}Al_{15}$ [29,30], whereas the β relaxation observed in $La_{70}Cu_{15}Al_{15}$ [29] is manifested in a shoulder only. Figure 2, in which the spectra are absolute and not normalized, and not broadened by the Cauchy-shaped frequency response obtained in DMA, clearly shows a difference in magnitude of both α and β relaxations between the alloys. Consequently, the pronounced β peak in the *normalized* loss modulus for $La_{70}Ni_{15}Al_{15}$, compared with $La_{70}Cu_{15}Al_{15}$, is a result of the relative magnitudes of the β and α relaxations.

By combining the standard linear solid model [26] and Eq. (1), STZ properties are obtained. The relaxation time constant (τ_m) for each STZ type, m, is determined as the median of the corresponding peak in Fig. 2, while each STZ volume (Ω_m) is obtained from the expression for the time constants [10,12],

$$\tau_m = \frac{3\eta'_m}{E'_m} = \frac{1}{\Omega_m \gamma_0^T} \cdot \frac{3kT}{2\mu(1+\nu)\gamma_0^c \nu_G} \cdot \exp\left(\mu\Omega_m \left\{\frac{\gamma_0^T}{kT}\left[\left(\frac{(7-5\nu)}{30(1-\nu)} + \frac{2(1+\nu)}{9(1-\nu)}\bar{\beta}^2\right)\gamma_0^T + \frac{1}{2}\frac{\overline{\sigma_{STZ}}}{\mu}\right]\right\}\right), \quad (4)$$

where η'_m and E'_m are effective viscosity and effective Young's modulus, respectively, of the Voigt Unit [26] associated with m-type STZs [12]. When employing Eq. (4) to obtain the STZ volumes, the shear modulus (μ) for each alloy composition is computed from the corresponding Young's modulus (E) by using $\mu = E/[2 \times (1+\nu)]$, and Young's modulus, E, is assumed to obey the rule of mixture [31],

$$E^{-1} = \sum_i f_i E_i^{-1}\,, \quad (5)$$

where f_i and E_i, i = 1,…3, are the atomic percentage and Young's modulus of each constituent element, respectively. The E_i values for La, Al, Ni and Cu are 37 GPa, 70 GPa, 200 GPa, and 130 GPa, respectively [32], which yields estimated values of 45 GPa and 46 GPa for $La_{70}Cu_{15}Al_{15}$ and $La_{70}Ni_{15}Al_{15}$, respectively. The latter is consistent with the measured value reported in Ref. [20], which validates the use of Eq. (5).

Figure 3 shows a comparison of τ_m (Fig. 3a) and Ω_m (Fig. 3b) between $La_{70}Cu_{15}Al_{15}$ and $La_{70}Ni_{15}Al_{15}$ for the STZ types that form in the kinetic window observed. In Fig. 3a, similar relaxation time constants are observed for both alloys, corresponding to the similar peak positions in Fig. 2. Figure 3b shows that when a uniform shear modulus is assumed, each alloy exhibits two regimes of STZ volume increments, indicated by the two fit lines. The slope difference between the fit lines for each alloy, ≈35%, is significant because the random error in Ω_m, which appears in the exponent in Eq. (4), is small. This difference cannot be attributed to the different measurement methods, since, for an Al-rich MG in Ref. [12], both regimes yielded the same slope and therefore STZ volume increment. For $La_{70}Cu_{15}Al_{15}$, the slope in the first regime, $0.153 \cdot 10^{-28}$ m^3, is close to the average atomic volume of Cu ($0.118 \cdot 10^{-28}$ m^3) and Al ($0.166 \cdot 10^{-28}$ m^3), which equals $0.142 \cdot 10^{-28}$ m^3, while the slope in the second regime, $0.206 \cdot 10^{-28}$ m^3, approximately equals the weighted average atomic volume, $0.219 \cdot 10^{-28}$ m^3, of Cu, Al and La ($0.372 \cdot 10^{-28}$ m^3). For $La_{70}Ni_{15}Al_{15}$, the slope in the first regime is $0.149 \cdot 10^{-28}$ m^3 and close to the average atomic volume, $0.138 \cdot 10^{-28}$ m^3, of Ni ($0.110 \cdot 10^{-28}$ m^3) and Al, while that in the second regime is $0.203 \cdot 10^{-28}$ m^3 and close to the average atomic volume of the alloy, $0.216 \cdot 10^{-28}$ m^3. Therefore, if a uniform shear modulus is assumed for each alloy, possibly distinct STZ compositions in the α and β regime,

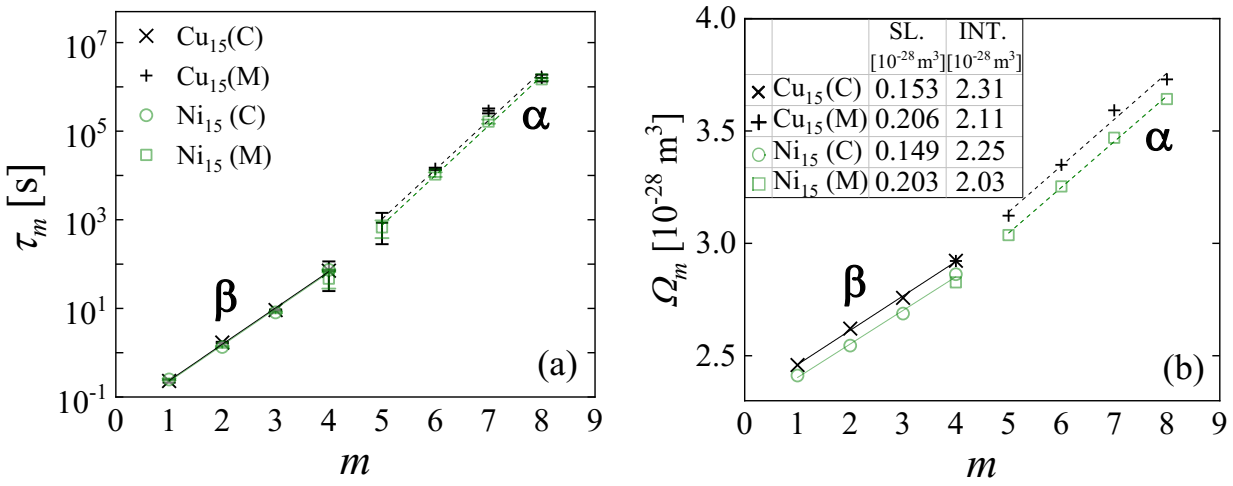

Figure 3. (a) Relaxation time constants (τ_m) determined as the median of each spectrum peak in Fig. 2 and (b) STZ volume (Ω_m) from Eq. (4) as a function of STZ type (m) for $La_{70}Cu_{15}Al_{15}$ (crosses and pluses, labeled "Cu_{15}") and $La_{70}Ni_{15}Al_{15}$ (circles and squares, labeled "Ni_{15}") aged at RT for $1.9 \cdot 10^6$ s. m = 1,…,4 (crosses and circles) correspond to cantilever bending (labeled "C"), while m = 4,…,8 (pluses and squares) correspond to mandrel measurements (labeled "M"). For each alloy, two regimes are revealed, with the solid and dashed lines being fit lines. The error bars for Ω_m are smaller than the symbols. The legend in Fig. 3b includes the details of the fit line with "SL." and "INT." corresponding to its slope and intercept, respectively.

which differ from the macroscopic average, are obtained for both $La_{70}Cu_{15}Al_{15}$ and $La_{70}Ni_{15}Al_{15}$, as we also reported for $La_{55}Ni_{20}Al_{25}$ MG [13].

Diffraction studies [33] and recent simulations [34] suggest that mesoscale structural heterogeneity is intrinsic to the glassy state. Microscopy results [6] suggest that a La-based MG is chemically heterogeneous. If the same is true for the present alloys, the two regimes in Fig. 3 could possibly be attributed to local variation in atomic size and/or in corresponding local modulus [23,24].

Moreover, our earlier observations [18] that only the properties of slow and large STZs are affected by aging or cryogenic cycling are consistent with the presence of domains with different structural relaxation kinetics.

Figure 4 shows the volume fraction of *m*-type PSTZs [12], Eq. (3), as a function of their activation free energy (ΔF_m, Eq. (2)) for shear transformation divided by kT, T = RT, for $La_{70}Cu_{15}Al_{15}$ and $La_{70}Ni_{15}Al_{15}$. The activation free energy is a function of both STZ volume and shear modulus. It is noted that all time constants for constraint-free relaxation for both alloys in Fig. 3a are smaller than the total constraining time. Furthermore, since the time constants of the standard linear solid model under constraint are smaller than those for constraint-free relaxation, we conclude that all observed STZ types had reached mechanical equilibrium at the end of constraining period, and Eq. (3) is applicable.

For $La_{70}Cu_{15}Al_{15}$, c_m increases monotonically with increasing m and corresponding activation energy. However, for $La_{70}Ni_{15}Al_{15}$, a peak occurs at small ΔF_m values, similar to that for $La_{55}Ni_{20}Al_{25}$ in Ref. [13]. When comparing the two alloys, noticeable differences in c_m are observed for $\Delta F_m/\mathrm{k}T < 35$ and $\Delta F_m/\mathrm{k}T > 40$, which correspond to the β and α relaxations, respectively. The c_m values are larger for $La_{70}Ni_{15}Al_{15}$ than for $La_{70}Cu_{15}Al_{15}$ at lower activation energy, while the reverse holds at higher activation energy. This indicates that $La_{70}Ni_{15}Al_{15}$ possesses a larger volume fraction of fast and small PSTZs, while the volume fraction of slow and large PSTZs is larger in $La_{70}Cu_{15}Al_{15}$. In Ref. [6], the authors proposed that MGs with pronounced β relaxation may possess abundant PSTZs. Since a quantized hierarchy of STZs is obtained for both MGs with and without strong β relaxation in the present study, further details can be added –

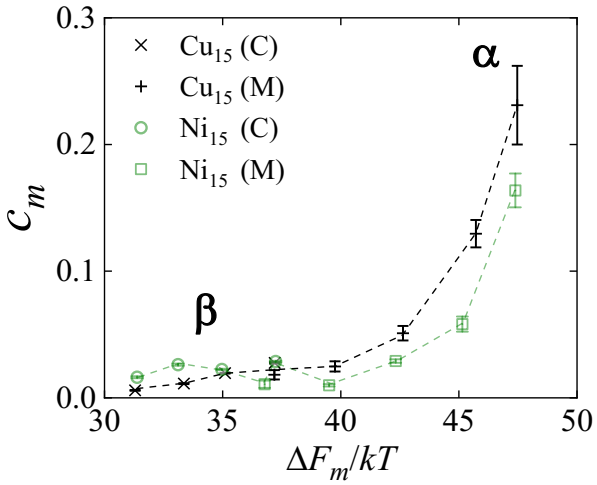

Figure 4. Volume fraction occupied by PSTZs for $La_{70}Cu_{15}Al_{15}$ (crosses and pluses, labeled "Cu_{15}") and $La_{70}Ni_{15}Al_{15}$ (circles and squares, labeled "Ni_{15}") with a RT aging time of $1.9 \cdot 10^6$ s as a function of their activation free energy for shear transformation divided by kT, T = RT. The error bars for $\Delta F_m/kT$ are smaller than the symbols. For m = 4, cantilever bending (labeled "C") and mandrel (labeled "M") measurements yield slightly different values of c_m and $\Delta F_m/kT$, which may be due to the limitation of the standard linear solid model used in the analysis.

MGs with pronounced β relaxation have more small and fast PSTZs than those with a weaker β peak, but having fewer large and slow PSTZs also contributes to the prominence of the β peak. The RT time constants corresponding to the small vs. large PSTZs are $\lesssim$ 10 s vs. $\gtrsim 10^4$ s-10^5 s, respectively.

Reference [6] reported a correlation between a pronounced β peak and large macroscopic plasticity, as a La-based MG with a stronger β relaxation exhibited greater plasticity than other MGs, e.g., Zr-based alloys. We observe here an opposite trend: Figure 5 shows representative RT tensile tests at several strain rates. It shows consistently much larger plasticity for $La_{70}Cu_{15}Al_{15}$ than for

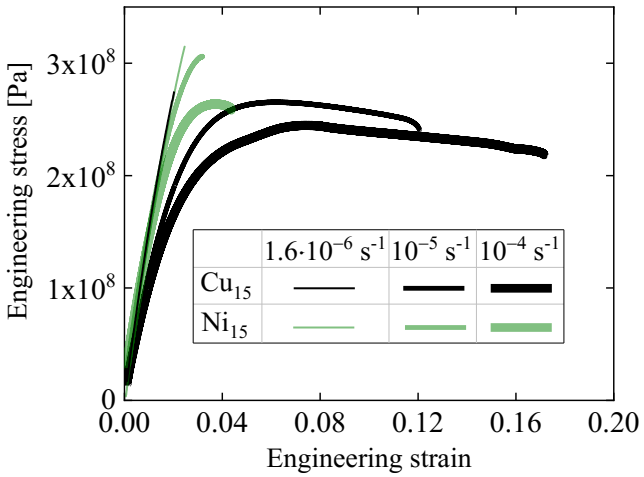

Figure 5. Engineering stress vs. engineering strain for $La_{70}Cu_{15}Al_{15}$ and $La_{70}Ni_{15}Al_{15}$ obtained from room-temperature tensile tests at strain rates of $1.6 \cdot 10^{-6}$ s^{-1}, 10^{-5} s^{-1}, and 10^{-4} s^{-1}. Curve thickness decreases with increasing strain rates. Each curve consists of 200-20,000 data points, depending on rate.

$La_{70}Ni_{15}Al_{15}$. The strong rate dependence is indicative of thermally activated deformation. The correlation between the anelastic relaxation behavior and plasticity is discussed next.

An estimate of the strain rate, based on the stress observed in Fig. 5 and presently obtained STZ properties, shows much smaller values than those imposed in Fig. 5. This is not surprising since the anelastic relaxation measurements were performed at small strain and therefore non-interacting STZs. The tensile measurements were carried out to higher strain, when the STZs occupy large volume fractions and their strain field therefore lowers the barriers for neighboring PSTZs. Thus, m=8 and possibly larger STZs can form at room temperature. The lower the applied strain rate, the higher the maximum size and time constant of STZs that contribute to deformation (See further discussion below). It should be noted that the apparent Young's modulus values in Fig. 5 for both

alloys are strain-rate dependent and smaller by a factor of ~ 3 than those used for obtaining STZ volumes, which were determined from ultrasonic experiments [32]. The main contribution to this difference is likely due to geometric imperfections. A reduction of about 10% is contributed by small and fast STZs, as estimated from their properties [12] for the stress values in Fig. 5.

The STZ spectra can be used qualitatively to explain the tensile behavior. With increasing strain and STZ density, each STZ slightly lowers the elastic barrier for surrounding PSTZs, resulting in reduced time constants and macroscopically homogeneous deformation. It is important to note that the term "homogeneous deformation" [2] is used in the literature to describe an activated flow state in which the structure is at a repeatedly regenerated steady state [8]. In contrast, we suggest that Fig. 5 reflects a transient state that persist until the remaining PSTZs in the inherent structure no longer keep up with the applied strain rate. The elastic energy is then released by localized deformation and failure. $La_{70}Cu_{15}Al_{15}$ has overall a higher density of PSTZs (Eq. 3) so that transient homogeneous deformation persists to higher strain. In contrast, the same extension rate is only accommodated in $La_{70}Ni_{15}Al_{15}$ by uniformly distributed STZs to a lower strain, and its stress therefore rises to higher values (Fig. 5).

We note that the glass transition of $La_{70}Cu_{15}Al_{15}$, 391 K, is lower than that of $La_{70}Ni_{15}Al_{15}$, 431 K, corresponding to homologous temperatures of 0.75 and 0.68, respectively. Thus, one expects a higher rate of thermally activated shear transformations for the former. Indeed, this argument is analogous to that based on the present spectra. With increasing temperature, increasingly larger PSTZs contribute to deformation, and the glass transition is reached when the rigid part of the solid

no longer percolates. With a higher concentration of PSTZs, $La_{70}Cu_{15}Al_{15}$ is expected to reach this point at a lower temperature.

The present observations suggest that the relative intensity of the β relaxation may not be a reliable screening criterion in the development of MGs with large plasticity. We suggest that the total normalized anelastic strain at short time after constraint removal, $\varepsilon_{an}(t \to 0)/\varepsilon_{el}^{0}$ in Fig. 1(b), can serve for screening alloys for their plasticity. It is equal to the integrated area of the spectrum (Fig. 2(b)).

Conclusions

A detailed description of the composition effect on both α and β relaxations is provided by comparing STZ properties of $La_{70}Cu_{15}Al_{15}$ and $La_{70}Ni_{15}Al_{15}$ from anelastic relaxation, ranging from less than one second to more than one year. The pronounced β relaxation in normalized DMA data, observed in $La_{70}Ni_{15}Al_{15}$ but not in $La_{70}Cu_{15}Al_{15}$, is due to both the larger volume fraction of fast and small *potential* STZs, corresponding to the β relaxation, and the smaller volume fraction of slow and large *potential* STZs, corresponding to the α relaxation, in the former alloy. The connection between anelastic relaxation behavior and macroscopic plasticity is examined by performing quasi-static room-temperature tensile tests on both alloys. The degree of plasticity is strongly rate dependent. $La_{70}Cu_{15}Al_{15}$ exhibits larger plasticity than $La_{70}Ni_{15}Al_{15}$, a trend opposite to a previously reported correlation between strong β relaxation and large plasticity. The present anelasticity data qualitatively explain the observed plasticity. Using the loss modulus as a screening tool for plasticity would require absolute measurements and consideration of the intensities of both α and β relaxations.

Acknowledgements

This work was funded by the U.S. National Science Foundation (NSF), Grants Nos. DMR-1307884 and DMR-1708043. The authors are grateful to Professor Kenneth Kozloff for the use of the nanoindenter in his laboratory.

References

[1] C. A. Schuh, T. C. Hufnagel, and U. Ramamurty, Mechanical behavior of amorphous alloys, Acta Mater. 55 (2007) 4067-4109.

[2] F. Spaepen, A microscopic mechanism for steady state inhomogeneous flow in metallic glasses, Acta Metall. 25 (1977) 407-415.

[3] A. L. Greer and E. Ma, Bulk metallic glasses: At the cutting edge of materials research, MRS Bull. 32 (2007) 611-619.

[4] H. B. Yu, W. H. Wang, and K. Samwer, The β relaxation in metallic glasses: an overview, Mater. Today 16 (2013) 183-191.

[5] J. Qiao, J. -M. Pelletier, and R. Casalini, Relaxation of Bulk Metallic Glasses Studied by Mechanical Spectroscopy, J. Phys. Chem. B 117 (2013) 13658-13666.

[6] H. B. Yu, X. Shen, Z. Wang, L. Gu, W. H. Wang, and H. Y Bai, Tensile Plasticity in Metallic Glasses with Pronounced β relaxations, Phys. Rev. Lett. 108 (2012) 015504.

[7] H. B. Yu, W. H. Wang, H. Y. Bai, Y. Wu, and M. W. Chen, Relating activation of shear transformation zones to β relaxations in metallic glasses, Phys. Rev. B 81 (2010) 220201.

[8] A. S. Argon, Plastic deformation in metallic glasses, Acta Metall. 27 (1979) 47-58.

[9] M. L. Falk and J. S. Langer, Dynamics of viscoplastic deformation in amorphous solids, Phys. Rev. E 57 (1998) 7192.

[10] J. D. Ju and M. Atzmon, Atomistic interpretation of the dynamic response of glasses, MRS Commun. 4 (2014) 63-66.

[11] J. D. Ju and M. Atzmon, A comprehensive atomistic analysis of the experimental dynamic-mechanical response of a metallic glass, Acta Mater. 74 (2014) 183-188.

[12] J. D. Ju, D. Jang, A. Nwankpa, and M. Atzmon, An atomically quantized hierarchy of shear transformation zones in a metallic glass, J. Appl. Phys. 109 (2011) 053522.

[13] T. J. Lei, L. Rangel DaCosta, M. Liu, W. H. Wang, Y. H. Sun, A. L. Greer, and M. Atzmon, Shear transformation zone analysis of anelastic relaxation of a metallic glass reveals distinct properties of α and β relaxations, Phys. Rev. E 100 (2019) 033001.

[14] A. Inoue, H. Yamaguchi, T. Zhang, and T. Masumoto, Al-La-Cu amorphous alloys with a wide supercooled liquid region, Mater. Trans. JIM 31 (1990) 104-109.

[15] A. Inoue, T. Zhang, and T. Masumoto, Al-La-Ni amorphous alloys with a wide supercooled liquid region, Mater. Trans. JIM 30 (1989) 965-972.

[16] X. D. Wang, B. Ruta, L. H. Xiong, D. W. Zhang, Y. Chushkin, H. W. Sheng, H. B. Lou, Q. P. Cao and J. Z. Jiang, Free-volume dependent atomic dynamics in beta relaxation pronounced La-based metallic glasses, Acta Mater. 99 (2015) 290-296.

[17] H. B. Yu, K. Samwer, W. H. Wang, and H. Y. Bai, Chemical influence on β-relaxations and the formation of the molecule-like metallic glasses, Nat. Commun. 4 (2013) 2204.

[18] T. J. Lei, L. Rangel DaCosta, M. Liu, W. H. Wang, Y. H. Sun, A. L. Greer, and M. Atzmon, Microscopic characterization of structural relaxation and cryogenic rejuvenation in metallic glasses, Acta Mater. 164 (2019) 165-170.

[19] A. S. Argon, Strain avalanches in plasticity, Philos. Mag. 93 (2013) 3795-3808.

[20] S. T. Liu, Z. Wang, H. L. Peng, H. B. Yu, and W. H. Wang, The activation energy and volume of flow units of metallic glasses, Scr. Mater. 67 (2012) 9-12.

[21] A. S. Argon and L. T. Shi, Development of visco-plastic deformation in metallic glasses, Acta Metall. 31 (1983) 499-507.

[22] H. Kato, H. Igarashi, and A. Inoue, Another clue to understand the yield phenomenon at the glassy state in Zr55Al10Ni5Cu30 metallic glass, Mater. Lett. 62 (2008) 1592-1594.

[23] H. Wagner, D. Bedorf, S. Küchemann, M. Schwabe, B. Zhang, W. Arnold, and K. Samwer, Local elastic properties of a metallic glass, Nat. Mater. 10 (2011) 439-442.

[24] P. Tsai, K. Kranjc, and K. M. Flores, Hierarchical heterogeneity and an elastic microstructure observed in a metallic glass alloy, Acta Mater. 139 (2017) 11-20.

[25] E. Orowan, Proceedings of the first national congress of applied mechanics 453 (1952).

[26] A. S. Nowick and B. S. Berry, Anelastic Relaxation in Crystalline Solids (Academic, New York 1972).

[27] S. W. Provencher, A constrained regularization method for inverting data represented by linear algebraic or integral equations, Comput. Phys. Commun. 27 (1982) 213.

[28] S. W. Provencher, CONTIN: a general purpose constrained regularization program for inverting noisy linear algebraic and integral equations, Comput. Phys. Commun. 27 (1982) 229.

[29] Z. Wang, H. B. Yu, P. Wen, H. Y. Bai, and W. H. Wang, Pronounced slow β-relaxation in La-based bulk metallic glasses, J. Phys.: Condens. Matter 23 (2011) 142202.

[30] H. Okumura, H. S. Chen, A. Inoue, and T. Masumoto, Sub-T_g mechanical relaxation of a $La_{55}Ni_{20}Al_{25}$ amorphous alloy, J. Non-Cryst. Solids 130 (1991) 304-310.

[31] Z. Zhang, R. J. Wang, L. Xia, B. C. Wei, D. Q. Zhao, M. X. Pan, and W. H. Wang, Elastic behavior and microstructural characteristics of $Nd_{60}Al_{10}Fe_{20}Co_{10}$ bulk metallic glass investigated by ultrasonic measurement under pressure, J. Phys.: Condens. Matter 15 (2003) 4503-4509.

[32] W. H. Wang, The elastic properties, elastic models and elastic perspectives of metallic glasses, Prog. Mater. Sci. 57 (2012) 487-656.

[33] W. Dmowski, T. Iwashita, C.-P. Chuang, J. Almer, and T. Egami, Elastic Heterogeneity in Metallic Glasses, Phys. Rev. Lett. 105 (2010) 205502.

[34] Q. An, W. L. Johnson, K. Samwer, S. L. Corona, and W. A. Goddard, III, First-order phase transition in liquid Ag to the heterogeneous G-phase, J. Phys. Chem. Lett. 11 (2020) 632-645.